Journal of
Applied and Computational Mechanics

M&MoCS

Shahid Chamran
University of Ahvaz

Research Paper

Time-Discontinuous Finite Element Analysis of Two-Dimensional Elastodynamic Problems using Complex Fourier Shape Functions

Ebrahim Izadpanah, Saeed Shojaee, Saleh Hamzehei-Javaran

Civil Engineering Department, Shahid Bahonar University of Kerman, Kerman, Iran

Abstract. This paper reformulates a time-discontinuous finite element method (TD-FEM) based on a new class of shape functions, called complex Fourier hereafter, for solving two-dimensional elastodynamic problems. These shape functions, which are derived from their corresponding radial basis functions, have some advantages such as the satisfaction of exponential and trigonometric function fields in complex space as well as the polynomial ones simultaneously, that make them a better choice than classic Lagrange shape functions, which only can satisfy polynomial function field. To investigate the validity and accuracy of the proposed method, three numerical examples are provided and the results obtained from the present method (complex Fourier-based TD-FEM) and the classic Lagrange-based TD-FEM are compared with the exact analytical solutions. According to them, using complex Fourier functions in TD-FEM leads to more accurate and stable solutions rather than those obtained from the classic TD-FEM.

Keywords: Time-discontinuous finite element method; Two-dimensional elastodynamic analysis; Complex Fourier shape functions; Radial basis functions.

1. Introduction

In general, the formulation of many natural phenomena, such as earthquake, is done through a set of partial differential equations and solved by its corresponding analytical solution. However, solving analytically is not always possible due to some difficulties. For solving this problem, n ... The most common numerical methods used nowadays are finite element method, isogeometric method, boundary element method and different kinds of mesh-less methods. The accuracy, efficiency and time cost are the three most important factors in choosing a numerical method.

Among the most interesting problems considered by researchers, elastodynamic can be pointed out. To solve this problem numerically, many methods have been suggested. One of them is semi-discrete finite element method, which first, by using finite elements in spatial domain, the governing partial differential equation is reduced to a time dependent system of ordinary differential equations. Then, they can be solved using the traditional direct time integration methods, such as Newmark or finite difference methods. However, one of the most important disadvantages of this approach is its inefficiency in problems with high-frequency or sharp gradients in solution. The impact of a bar against a rigid wall is an important example about this matter discussed by Hulbert and Hughes (1990). They solved the problem using a semi-discrete approach (finite element in space, trapezoidal rule algorithm in time) and showed that there are significant oscillations in the solution. They improved the solution by using the Hilber-Hughes-Taylor-α (HHT-α) method instead of the traditional trapezoidal rule. In recent decades, many other efforts have been made to solve this issue from the semi-discrete approach viewpoint (Hilber et al. 1977; Chung and Hulbert 1993; Shao and Cai 1988; Fung 1999; Tamma et al. 2001; Zhou and Tamma 2004; Bathe and Baig 2005).

Another method for obtaining suitable results in elastodynamic problems is space-time finite element. This method considers time as an additional dimension and discretizes it using known finite elements (e.g. a two dimensional problem is changed to a three dimensional one (two dimensions in space and one dimension in time) from the space-time finite element viewpoint). Argyris and Scharpf (1969) were the first researchers to employ this method. In their work, the equation of motion of a mass point was considered and finite elements were applied in time to get the system of algebraic equations. Similar works have been also done by Fried (1969), Oden (1969), Wilson (1966) and Zienkiewicz (1970;1977;1977).

In a general classification, the space-time finite element methods are categorized into two groups; namely time-continuous and time-discontinuous finite element method. In the first one, unknown variables areconsidered to be continuous with respect to time, which leads to the formation of a coupled matrix system. When this system is solved, the solution will be achieved at all locations and all times. Various engineering problems have been solved by using this method (Varoglu and Finn 1980; Nguyen and Reynen 1984; Lewis et al. 1987; Peters and Izadpanah 1988; Bruch and Zyvoloski 1974; Dyniewicz 2014; Saedpanah 2013; Tang et al. 2006). However, in time-discontinuous finite element method, unknown quantities can have different values at a given time, unlike the time-continuous one. In the early 1970s, this approach was first proposed and analyzed as a technique for solving partial differential equations numerically. As examples for the application of this method, Reed and Hill (1973) employed it for solving the hyperbolic neutron transport equation, similar to the work of Lesaint and Raviart (1974). Hughes and Hulburt (1988) applied this method for solving elastodynamic problems. In their work, time-discontinuous finite element method was combined with stabilizing terms of least-square type and a mathematical analysis was performed to prove that the method converges at the optimal rate in a norm stronger than the total energy norm. Later, Hulbert (1992) utilized similar stabilizing terms for structural dynamics by developing two general formulations: single-field and double-field, and their convergence and stability were proved. More studies are reported in the literature about the usage of time-discontinuous approach for solving various engineering problems (Chien and Wu 2000; Li et al. 2003; Liu et al. 2008; Petersen et al. 2009; Aksoy and Senocak 2011; Guo et al. 2014).

In this study, a new class of shape functions are employed to be used in time-discontinuous finite element method for solving elastodynamic problems. The proposed functions are called complex Fourier shape functions and are used instead of classic Lagrange ones because of their advantages such as satisfying exponential, trigonometric and polynomial function fields in complex space simultaneously. It is worthwhile to mention that classic Lagrange shape functions are only able to satisfy polynomial function field. Khaji and Hamzehei Javaran (2013), and Hamzehei Javaran and Khaji (2014) employed complex Fourier functions for potential problems as well as the dynamic analysis of plane elasticity using boundary element method and the obtained results were interesting. According to their results, these shape functions are much more superior than classic Lagrange ones. To sum up, the idea of using the efficient complex Fourier shape functions in time-discontinuous finite element method for solving elastodynamic problems is investigated here.

This paper is configured as follows: Section 2 presents the system of governing differential equations of elastodynamic problems and derives concisely the corresponding weak formulation. The formulation and properties of complex Fourier Radial Basis Functions (RBFs) are discussed in detail in section 3 and the desired shape functions are derived through an enrichment technique. In section 4, the discretization process is explained. In the end, the accuracy and superiority of the suggested method are investigated through three numerical examples and the results are compared with analytical solutions and those obtained by classic time-discontinuous finite element method.

2. The formulation of Time-discontinuous finite element for elastodynamic problems

As a preliminary to this section, consider an elastic body in 2D space with region Ω and boundary Γ under some external tractions $(T(\Gamma_N, t))$ on Neumann boundaries (Γ_N) and supported on Dirichlet boundaries (Γ_D) (Fig. 1). The following equation is the dynamic equilibrium equation for this body:

$$\frac{\partial \sigma_x}{\partial x} + \frac{\partial \tau_{xy}}{\partial y} + f_{bx} = \rho \frac{\partial v_x}{\partial t}$$

$$\frac{\partial \tau_{xy}}{\partial x} + \frac{\partial \sigma_y}{\partial y} + f_{by} = \rho \frac{\partial v_y}{\partial t}$$

$$\rho v_x = \rho \frac{\partial u_x}{\partial t}$$

$$\rho v_y = \rho \frac{\partial u_y}{\partial t}$$

(1)

in which, σ_x, σ_y, and τ_{xy} denote the stress tensor components in 2D space. f_{bx} and f_{by} are body forces in x and y directions, respectively and they are assumed to be constant over time. $\mathbf{u} = [u_x(\Omega, t) \ u_y(\Omega, t)]^T$ and $\mathbf{v} = [v_x(\Omega, t) \ v_y(\Omega, t)]^T$ represent displacement and velocity vectors of any particle at time t, respectively. Moreover, ρ denotes the mass per unit volume assumed to be the same for the whole region Ω. The boundary conditions are as below:

$$\sigma_x n_x + \tau_{xy} n_y = T_x(\Gamma_N, t) \quad \text{on } \Gamma_N$$
$$\tau_{xy} n_x + \sigma_y n_y = T_y(\Gamma_N, t) \quad \text{on } \Gamma_N$$
$$\mathbf{u}(\Gamma_D, t) = \mathbf{g}_u(\Gamma_D, t) \quad \text{on } \Gamma_D$$
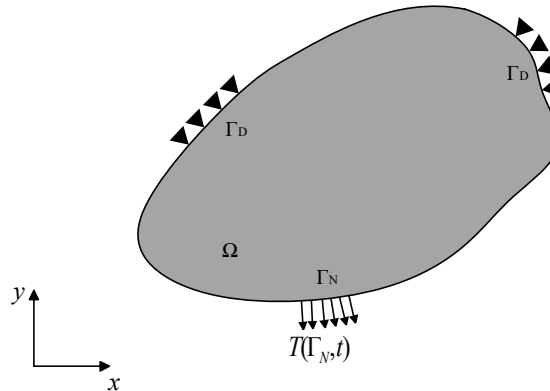$$\mathbf{v}(\Gamma_D, t) = \mathbf{g}_v(\Gamma_D, t) \quad \text{on } \Gamma_D$$

(2)

Fig. 1. A sample of two-dimensional elastic body

in which, n_x and n_y denote the unit outward normal vector components to the Γ_N in x and y directions, respectively. T_x and T_y are the traction vector components; $\mathbf{g}_u$ and $\mathbf{g}_v$ represent the prescribed displacements and velocities on Γ_D. The initial conditions are as follows:

$$\mathbf{u}(\Omega, 0) = \mathbf{u}_0(\Omega)$$
$$\mathbf{v}(\Omega, 0) = \mathbf{v}_0(\Omega)$$

(3)

where, $\mathbf{u}_0$ and $\mathbf{v}_0$ denote displacements and velocities of the body at the initial time. Substituting the stress-strain and strain-displacement relationships into Eq. (1) cause the system of partial differential equations to be represented in terms of displacements and velocities, which is known as the two-variable formulation of elastodynamic problem. Consider $I = [0, T]$, a time interval divided into n segments, each one called a time slab and denoted by $I_n = [t_{n-1}, t_n]$, in the form of $0 = t_0 < t_1 < \ldots\ldots < t_n = T$. In Fig. 2, a sample of space-time discretization using 3D elements that consists of two elements in space domain is illustrated. Multiplying Eq. (1) in the trial function (W) and integrating in space (Ω) and time slab (I_n) leads to obtaining the weak form of Eq. (1) as below:

$$\int_{I_n}\int_{\Gamma_N} W \, T_x \, d\Gamma dt - \int_{I_n}\int_{\Omega} \nabla W \cdot \begin{bmatrix} \sigma_x \\ \tau_{xy} \end{bmatrix} d\Omega dt + \int_{I_n}\int_{\Omega} W \, f_{bx} \, d\Omega dt - \int_{I_n}\int_{\Omega} \rho W \, \frac{\partial v_x}{\partial t} d\Omega dt +$$
$$C\int_{\Omega} W(\Omega, t_{n-1}^+)\,[v_y(\Omega, t_{n-1})]\,d\Omega = 0$$

(4)

$$\int_{I_n}\int_{\Gamma_N} W \, T_y \, d\Gamma dt - \int_{I_n}\int_{\Omega} \nabla W \cdot \begin{bmatrix} \tau_{xy} \\ \sigma_y \end{bmatrix} d\Omega dt + \int_{I_n}\int_{\Omega} W \, f_{by} \, d\Omega dt - \int_{I_n}\int_{\Omega} \rho W \, \frac{\partial v_y}{\partial t} d\Omega dt +$$
$$C\int_{\Omega} W(\Omega, t_{n-1}^+)\,[v_x(\Omega, t_{n-1})]\,d\Omega = 0$$

(5)

$$\int_{I_n}\int_{\Omega} \rho W \, v_x \, d\Omega dt - \int_{I_n}\int_{\Omega} \rho W \, \frac{\partial u_x}{\partial t} d\Omega dt + C\int_{\Omega} W(\Omega, t_{n-1}^+)\,[u_y(\Omega, t_{n-1})]\,d\Omega = 0$$

(6)

$$\int_{I_n}\int_{\Omega} \rho W \, v_y \, d\Omega dt - \int_{I_n}\int_{\Omega} \rho W \, \frac{\partial u_y}{\partial t} d\Omega dt + C\int_{\Omega} W(\Omega, t_{n-1}^+)\,[u_x(\Omega, t_{n-1})]\,d\Omega = 0$$

(7)

In Eqs. (4)-(7), the last terms apply the continuity of displacement and velocity at time $t = t_{n-1}$ in a weak way and they are neglected at the first time slab because there is no need for the displacement and velocity to be continuous at $t = t_0$. Moreover, the penalty coefficient C, should be chosen large enough to make sure that the continuity of displacement and velocity is appropriately satisfied. $[A(\Omega, t_n)]$ is the jump operator in time and is defined below:

$$[A(\Omega, t_n)] = A(\Omega, t_n^+) - A(\Omega, t_n^-)$$

(8)

in which,

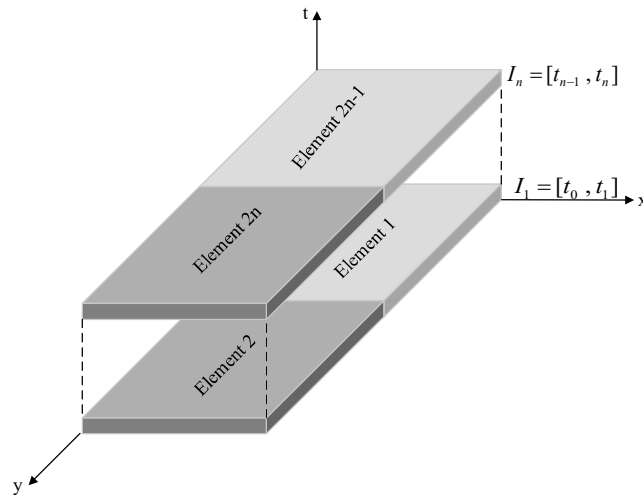$$A(\Omega, t_n^\pm) = \lim_{\varepsilon \to 0^\pm} A(\Omega, t + \varepsilon)$$

(9)

Fig. 2. A sample of space-time discretization using three-dimensional elements

In order to obtain the matrix form of Eqs. (4)-(7), the displacement, velocity and trial functions should be approximated by linear combination of suitable shape functions multiplied by unknown nodal values. The well-known classic Lagrange functions are common shape functions in space-time finite element methods. However, in this paper, these functions are replaced with complex Fourier ones. The next section describes the formulation and properties of complex Fourier shape functions.

3. Proposed complex Fourier shape functions

This section introduces the complex Fourier functions as suitable and efficient shape functions to be used in space-time finite element method. Due to the oscillating and decaying features of complex Fourier shape functions, they are suitable for modelling wave in elastodynamic problems and being used in wave propagation ones. In the beginning, a radial basis function (RBF) containing the combination of the trigonometric and exponential functions in complex space is presented. According to the concept of complex Fourier series, any piecewise continuous function $\overline{P}(r)$ can be expressed as below:

$$\overline{P}(r) = \sum_{s=-\infty}^{+\infty} c_s e^{i\omega_s r} \tag{10}$$

in which, c_s and ω_s are the common parameters of complex Fourier series. Now, let us consider only one term of Eq. (10) so that complex Fourier RBF is defined as below:

$$R(r) = a\, e^{i\omega r} \tag{11}$$

where, $i^2 = -1$. Moreover, a and ω are the shape parameters and choosing them wisely plays a significant role in the accuracy of the method. In the following, the enrichment process of complex Fourier radial basis functions and obtaining the final form of shape functions is discussed in details.

3.1 Enrichment of complex Fourier radial basis function

The enrichment process of complex Fourier RBF is presented for a 1D three-node element in this section. The function $\phi(\mathbf{x})$ can be approximated using the mentioned RBF and polynomial functions as below:

$$\phi(\mathbf{x}) \simeq \phi_h(\mathbf{x}) = \sum_{s=1}^{nr} R_s(r)\, \alpha_s + \sum_{t=1}^{np} P_t(\mathbf{x})\, \beta_t \tag{12}$$

in which, $R_s(r)$ and $P_t(\mathbf{x})$ denote the sth radial basis function and tth polynomial basis function, respectively; nr and np represent the number of nodes and basis polynomial terms. It is worthwhile to mention that the maximum number of polynomial functions that can be used for the enrichment is $nr-1$. A re-written form of Eq. (12) is provided in the following:

$$\begin{aligned}
\phi_h(\mathbf{x}) &= \mathbf{R}^T\boldsymbol{\alpha} + \mathbf{P}^T\boldsymbol{\beta} \\
\mathbf{R} &= [R_1 \quad R_2 \quad \dots \quad R_{ne}]^T \\
\mathbf{P} &= [P_1 \quad P_2 \quad \dots \quad P_{np}]^T \\
\boldsymbol{\alpha} &= [\alpha_1 \quad \alpha_2 \quad \dots \quad \alpha_{ne}]^T \\
\boldsymbol{\beta} &= [\beta_1 \quad \beta_2 \quad \dots \quad \beta_{np}]^T
\end{aligned} \tag{13}$$

Satisfying Eq. (13) for all nodes leads to:

$$\overline{\phi} = \overline{\mathbf{R}}\,\alpha + \overline{\mathbf{P}}\,\beta \qquad (14)$$

where,

$$\overline{\phi} = \begin{bmatrix} \phi(\mathbf{x}_1) \\ \vdots \\ \phi(\mathbf{x}_n) \end{bmatrix} \quad , \quad \overline{\mathbf{R}} = \begin{bmatrix} R_1(r_1) & \cdots & R_n(r_1) \\ \vdots & \ddots & \vdots \\ R_1(r_n) & \cdots & R_n(r_n) \end{bmatrix} \quad , \quad \overline{\mathbf{P}} = \begin{bmatrix} P_1(\mathbf{x}_1) & \cdots & P_m(\mathbf{x}_1) \\ \vdots & \ddots & \vdots \\ P_1(\mathbf{x}_n) & \cdots & P_m(\mathbf{x}_n) \end{bmatrix} \qquad (15)$$

As it is seen, the number of unknowns in Eq. (14) is $nr + np$, while only nr equations exist. Therefore, np extra equations are needed to have a unique answer. It is shown that the following condition should be met to have a unique solution (Wang and Liu 2002)

$$\sum_{s=1}^{nr} P_t(\mathbf{x}_s)\,\alpha_s = 0 \quad , \quad t = 1, 2, ..., np \qquad (16)$$

The unknowns can be determined by solving the following system considering Eqs. (14) and (16):

$$\begin{bmatrix} \overline{\mathbf{R}} & \overline{\mathbf{P}} \\ \overline{\mathbf{P}}^T & \mathbf{0} \end{bmatrix} \begin{bmatrix} \alpha \\ \beta \end{bmatrix} = \begin{bmatrix} \overline{\phi} \\ \mathbf{0} \end{bmatrix} \qquad (17)$$

The vectors α and β can be expressed as below:

$$\alpha = \mathbf{Z}_\alpha\,\overline{\phi} \quad , \quad \beta = \mathbf{Z}_\beta\,\overline{\phi} \qquad (18)$$

$$\mathbf{Z}_\beta = [\overline{\mathbf{P}}^T\,\overline{\mathbf{R}}^{-1}\overline{\mathbf{P}}]^{-1}\overline{\mathbf{P}}^T\,\overline{\mathbf{R}}^{-1} \quad , \quad \mathbf{Z}_\alpha = \overline{\mathbf{R}}^{-1} - \overline{\mathbf{R}}^{-1}\overline{\mathbf{P}}\mathbf{Z}_\beta \qquad (19)$$

Finally, substituting Eq. (18) into Eq. (13) leads to obtaining the relationship between function field $\phi_h(\mathbf{x})$ and vector of nodal values $\overline{\phi}$ as below:

$$\phi_h(\mathbf{x}) = [\mathbf{R}^T(r)\mathbf{Z}_\alpha + \mathbf{P}^T(\mathbf{x})\mathbf{Z}_\beta]\,\overline{\phi} = \mathbf{N(x)}\overline{\phi} \qquad (20)$$

in which, $\mathbf{N(x)}$ represents the vector of shape functions. Now, the above mentioned process is implemented on a 1D three-node element in a natural coordinate system ξ (see Fig. 3a) and the shape functions corresponding to this element are obtained. Then, the shape functions of a 27-node cubic element, which is the desired element in this paper, will be obtained by extending the 1D functions in 3D natural coordinate system (ξ, η, ζ) (see Fig. 3b). The vector of radial basis functions and the polynomial functions of a 3-node element are defined as below:

$$\mathbf{R}(r) = \begin{bmatrix} R_1(r) \\ R_2(r) \\ R_3(r) \end{bmatrix} = \begin{bmatrix} a\,e^{i\omega|\xi+1|} \\ a\,e^{i\omega|\xi|} \\ a\,e^{i\omega|\xi-1|} \end{bmatrix} \qquad (21)$$

$$\mathbf{P}(\xi) = \begin{bmatrix} 1 \\ \xi \end{bmatrix} \qquad (22)$$

The matrices $\overline{\mathbf{R}}$ and $\overline{\mathbf{P}}$ are defined as follows:

$$\overline{\mathbf{R}} = a \begin{bmatrix} 1 & e^{i\omega} & e^{2i\omega} \\ & 1 & e^{i\omega} \\ Sym. & & 1 \end{bmatrix} \qquad (23)$$

$$\overline{\mathbf{P}} = \begin{bmatrix} 1 & -1 \\ 1 & 0 \\ 1 & 1 \end{bmatrix} \qquad (24)$$

Substituting Eqs. (23) and (24) into Eq. (19) leads to:

$$\mathbf{Z}_\alpha = \frac{1}{2a(1-e^{i\omega})(3-e^{i\omega})} \begin{bmatrix} 1 & -2 & 1 \\ & 4 & -2 \\ sym. & & 1 \end{bmatrix} \qquad (25)$$

$$\mathbf{Z}_\beta = \frac{1}{3-e^{i\omega}} \begin{bmatrix} 1 & 1-e^{i\omega} & 1 \\ -0.5(3-e^{i\omega}) & 0 & 0.5(3-e^{i\omega}) \end{bmatrix} \qquad (26)$$

Finally, the vector of shape functions is obtained as below for a 3-node element in the natural coordinate system ξ:

$$\mathbf{N}(\xi) = [N_1(\xi) \quad N_2(\xi) \quad N_3(\xi)] \tag{27}$$

$$N_1(\xi) = \frac{1}{2}(-\xi + c + k(\xi)) \tag{28}$$

$$N_2(\xi) = (1-c) - k(\xi) \tag{29}$$

$$N_3(\xi) = \frac{1}{2}(\xi + c + k(\xi)) \tag{30}$$

$$c = \frac{2}{3 - e^{i\omega}} \tag{31}$$

$$k(\xi) = \frac{e^{i\omega|\xi+1|} - 2e^{i\omega|\xi|} + e^{i\omega|\xi-1|}}{(1 - e^{i\omega})(3 - e^{i\omega})} \tag{32}$$

It should be noted that in the enrichment process, the shape parameter a vanishes and only the shape parameter ω remains. To obtain the shape functions of a 27-node cubic element, Eq. (27) should be written in three ξ, η and ζ directions and the resultant functions should be multiplied to each other:

$$\psi_m(\xi, \eta, \zeta) = N_s(\xi) \times N_t(\eta) \times N_k(\zeta) \quad , \quad s,t,k = 1,2,3 \quad , \quad m = 1,2,...,27 \tag{33}$$

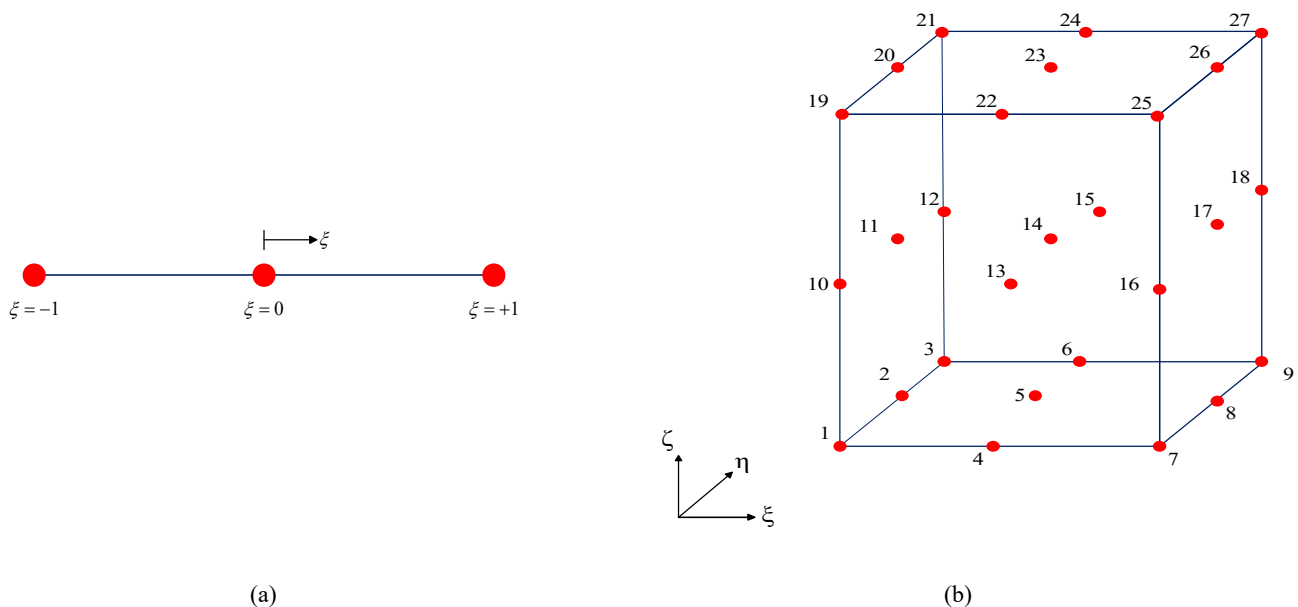(a)   (b)

Fig. 3. (a) A one-dimensional three-node complex Fourier element in natural space (b) A 27-node complex Fourier element in three-dimensional natural space

Some of the most important features of complex Fourier shape functions for a 1D 3-node element are expressed below. These properties can be easily expanded to 27-node element as well:

a) Kronecker delta property: If a shape function satisfies this property, its value equals one in its correspondence node and zero in other nodes. In other words:

$$N_m(\xi_n) = \begin{cases} 1 & m = n \\ 0 & m \neq n \end{cases} \tag{34}$$

Satisfying this property leads to having the same response in the points of the body as in its nodes. Moreover, the boundary conditions will be implemented more easily.

b) Partition of unity: The following equation can be easily obtained for a 1D 3-node complex Fourier element:

$$\sum_{j=1}^{3} N_j(\xi) = 1 \tag{35}$$

c) Infinite piecewise continuity: The first and higher order derivatives of the proposed shape functions are derived using the following relations:

$$\frac{d^m N_1(\xi)}{d\xi^m} = \frac{1}{2}(l + \frac{d^m k(\xi)}{d\xi^m}) \quad , \quad l = -1 \; if \; m = 1 \quad , \quad l = 0 \; if \; m = 2,3,...$$

$$\frac{d^m N_2(\xi)}{d\xi^m} = -\frac{d^m k(\xi)}{d\xi^m} \qquad , \quad m = 1,2,... \qquad\qquad\qquad (36)$$

$$\frac{d^m N_3(\xi)}{d\xi^m} = \frac{1}{2}(l + \frac{d^m k(\xi)}{d\xi^m}) \quad , \quad l = +1 \; if \; m = 1 \quad , \quad l = 0 \; if \; m = 2,3,...$$

According to the features of real-complex exponential functions, a recurrence relation can be obtained as below for calculating $k(\xi)$ derivatives:

$$\frac{d^m k(\xi)}{d\xi^m} = -\omega^2 \frac{d^{m-2} k(\xi)}{d\xi^{m-2}} \qquad\qquad\qquad (37)$$

d) Linear independence property: This property can be expressed as below for complex Fourier functions:

$$\sum_{j=1}^{3} c_j N_j(\xi; \xi_1, \xi_2, \xi_3) = 0 \quad \rightarrow \quad c_1 = c_2 = c_3 = 0 \qquad\qquad (38)$$

By replacing $\xi = \xi_k$ and using the Kronecker delta property, the above equation is proved as below:

$$0 = \sum_{n=1}^{3} c_n N_n(\xi_k) = \sum_{n=1}^{3} c_n \delta_{nk} \quad \rightarrow \quad c_n = 0 \, , n = 1,2,3 \qquad\qquad (39)$$

Some samples of the real part of complex Fourier shape functions of a one dimensional three-node element are plotted in Fig. 4. As it is shown in Figs. 4a and 4b, as the real part of shape parameter increases, more oscillations appear in the shape functions. It is due to the existence of trigonometric functions in the real part of the proposed shape functions. Also, Figs. 4c and 4d show that by choosing the higher imaginary part of ω, the behavior of the real part of proposed shape functions approaches to the exponential functions.
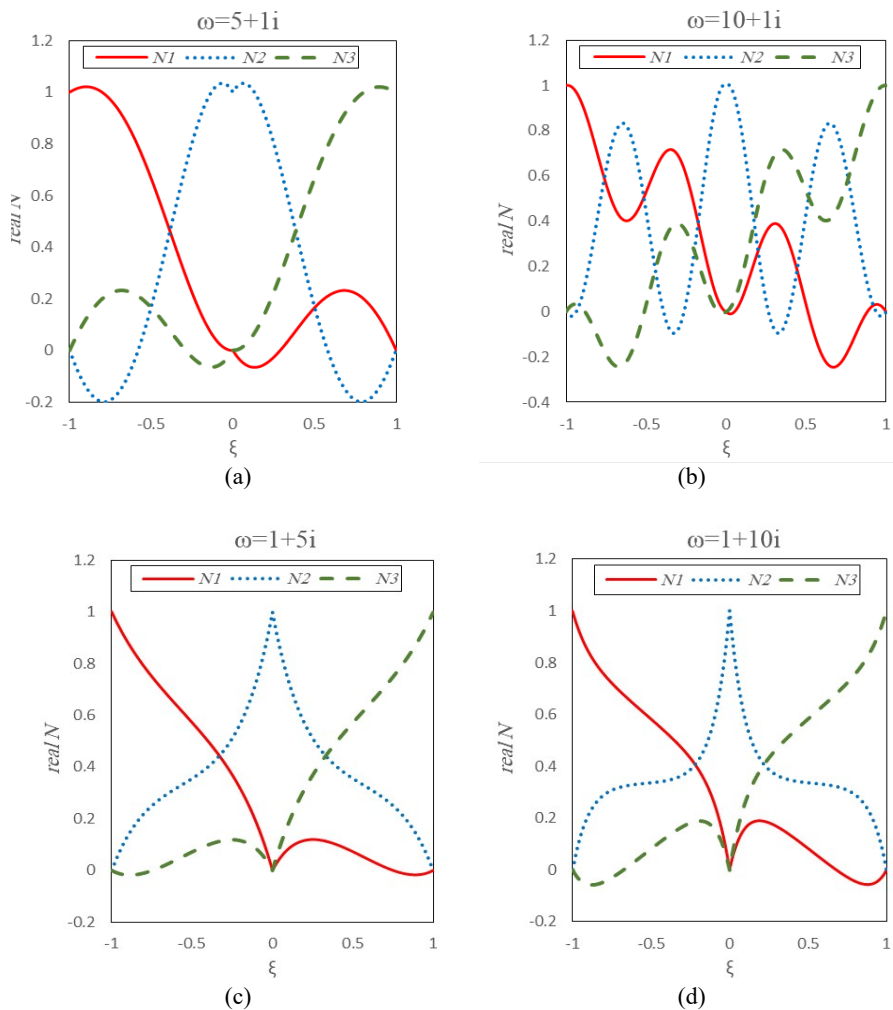
Fig. 4. The complex Fourier shape functions for a one dimensional three-node element

4. Discretization

The weak formulation of elastodynamic problems was achieved in section 2 (Eqs. (4)-(7)). Here, it is tried to approximate the displacement, velocity and trial functions using complex Fourier shape functions as the final step. To do so, the following relation can be used:

$$Z(\Omega,t) \simeq \psi(\Omega,t)\,\mathbf{z} \tag{40}$$

in which, $\psi(\Omega,t) = [\psi_1(\Omega,t) \quad \dots \quad \psi_{27}(\Omega,t)]$ denotes the vector of presented shape functions for a 27-node cubic element. $Z(\Omega,t)$ implies the desirable function for approximation (displacement, velocity and trial function), and $\mathbf{z}$ represents the nodal values vector corresponding to $Z(\Omega,t)$.

Substituting Eq. (40) into Eqs. (4)-(7) leads to obtaining the following matrix formulation:

$$\mathbf{K}\,\mathbf{d}^n = \mathbf{F}^{n-1} \tag{41}$$

$$\mathbf{K} = \begin{bmatrix} \mathbf{K}_{xx} & \mathbf{K}_{xy} & \mathbf{Q} & -C\mathbf{T}_1 \\ \mathbf{K}_{xy}^T & \mathbf{K}_{yy} & -C\mathbf{T}_1 & \mathbf{Q} \\ \mathbf{Q} & -C\mathbf{T}_1 & -\mathbf{M} & 0 \\ -C\mathbf{T}_1 & \mathbf{Q} & 0 & -\mathbf{M} \end{bmatrix}, \mathbf{d}^n = \begin{bmatrix} \mathbf{u}_x \\ \mathbf{u}_y \\ \mathbf{v}_x \\ \mathbf{v}_x \end{bmatrix}, \mathbf{F}^{n-1} = \begin{bmatrix} \mathbf{F}_{tx} + \mathbf{F}_{bx} - C\mathbf{T}_2\mathbf{V}_{y0} \\ \mathbf{F}_{ty} + \mathbf{F}_{by} - C\mathbf{T}_2\mathbf{V}_{x0} \\ -C\mathbf{T}_2\mathbf{U}_{y0} \\ -C\mathbf{T}_2\mathbf{U}_{x0} \end{bmatrix} \tag{42}$$

where, $\mathbf{U}_{x0}$ and $\mathbf{U}_{y0}$ denote the nodal displacement vectors in x and y directions obtained from the previous time slab, respectively. In a similar way, $\mathbf{V}_{x0}$ and $\mathbf{V}_{y0}$ represent the nodal velocity vectors. As discussed in section 2, C equals zero at the first time slab. Other parameters of Eq. (42) are defined as follows:

$$\mathbf{K}_{xx} = \int_{I_n}\int_\Omega \left(\frac{\partial \psi^T}{\partial x}D_1\frac{\partial \psi}{\partial x} + \frac{\partial \psi^T}{\partial y}D_2\frac{\partial \psi}{\partial y}\right)d\Omega dt \tag{43}$$

$$\mathbf{K}_{yy} = \int_{I_n}\int_\Omega \left(\frac{\partial \psi^T}{\partial y}D_1\frac{\partial \psi}{\partial y} + \frac{\partial \psi^T}{\partial x}D_2\frac{\partial \psi}{\partial x}\right)d\Omega dt \tag{44}$$

$$\mathbf{K}_{xy} = \int_{I_n}\int_\Omega \left(\frac{\partial \psi^T}{\partial x}D_3\frac{\partial \psi}{\partial y} + \frac{\partial \psi^T}{\partial y}D_2\frac{\partial \psi}{\partial x}\right)d\Omega dt \tag{45}$$

$$\mathbf{Q} = \int_{I_n}\int_\Omega \psi^T \rho \frac{\partial \psi}{\partial t}d\Omega dt \tag{46}$$

$$\mathbf{M} = \int_{I_n}\int_\Omega \psi^T \rho\, \psi\, d\Omega dt \tag{47}$$

$$\mathbf{F}_{tx} = \int_{I_n}\int_{\Gamma_N} \psi^T T_x\, d\Gamma dt \tag{48}$$

$$\mathbf{F}_{ty} = \int_{I_n}\int_{\Gamma_N} \psi^T T_y\, d\Gamma dt \tag{49}$$

$$\mathbf{F}_{bx} = \int_{I_n}\int_\Omega \psi^T f_{bx}\, d\Omega dt \tag{50}$$

$$\mathbf{F}_{by} = \int_{I_n}\int_\Omega \psi^T f_{by}\, d\Omega dt \tag{51}$$

$$\mathbf{T}_1 = \int_\Omega \psi^T(\Omega,t_{n-1}^+)\psi(\Omega,t_{n-1}^+)d\Omega \tag{52}$$

$$\mathbf{T}_2 = \int_\Omega \psi^T(\Omega,t_{n-1}^+)\psi(\Omega,t_{n-1}^-)d\Omega \tag{53}$$

In Eqs. (43-53), ψ represents the complex Fourier shape function matrix (see Eq. (33)), and D_1, D_2 and D_3 denote coefficients relating stress to strain and are defined as below for the plane stress case:

$$D_1 = \frac{E}{1-v^2} \quad , \quad D_2 = G \quad , \quad D_3 = vD_1 \tag{54}$$

and for the case of plane strain:

$$D_1 = \frac{E(1-v)}{(1+v)(1-2v)} \quad , \quad D_2 = G \quad , \quad D_3 = \frac{v}{1-v}D_1 \tag{55}$$

in which, E, G, and v denote young modulus, shear modulus, and Poisson ratio, respectively.

5. Numerical Examples

In order to assess the validity and accuracy of the proposed method, three numerical examples are provided here. The results of the present method are compared with analytical solutions as well as those of the classic time-discontinuous finite element. Before proceeding to the examples, there are some considerations that need to be taken :

    i.   The spatial and temporal domains are discretized using 3D 27-node cubic elements simultaneously.

    ii.   The value of penalty coefficient C is considered 10^4 .

    iii.   The effect of body forces is ignored.

5.1 A rectangular plate with a hole in its center

As the first example, a rectangular plate with the length of $36\,cm$ and width of $20\,cm$ is considered. There is a circular hole in the middle of this plate with the diameter of $10\,cm$ (Fig. 5a). Due to symmetry, only a quarter of the plate is modeled, as shown in Fig. 5b. In Fig. 5c, the discretization of the spatial domain using 16 elements is illustrated. The same pattern is also used for the time domain with 100 elements. The plate is subjected to a dynamic load in the form of $T_x(t) = 75\,H(t-0)\,MPa$, $H(t)$ denotes the Heaviside function, in its right and left sides (Fig. 5d). The material properties are as follows: $E = 2.1 \times 10^5\,MPa$, $v = 0.3$, and $\rho = 0.00785\,kg/cm^3$. In Fig. 6, the vertical displacement time story of point A is illustrated.
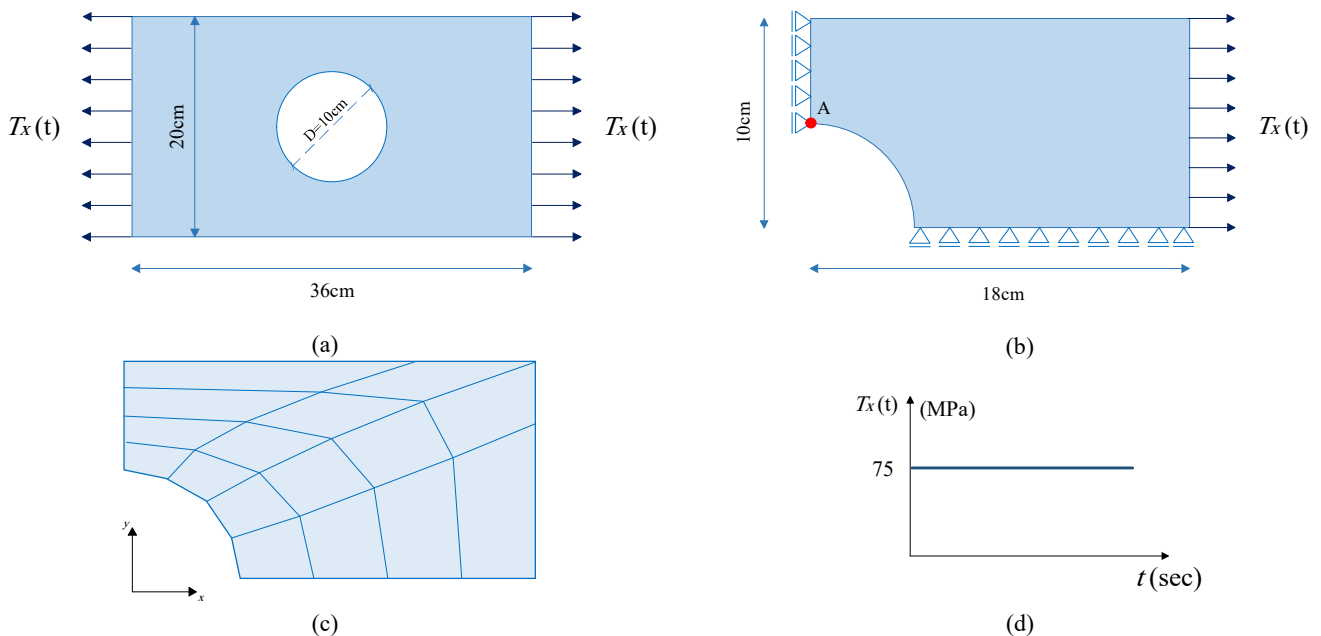
Fig. 5. (a) Geometry and loading of the perforated rectangular plate (b) Dimensions and boundary conditions used in the analysis (c) The discretization of spatial domain (d) The variation of loading with respect to time
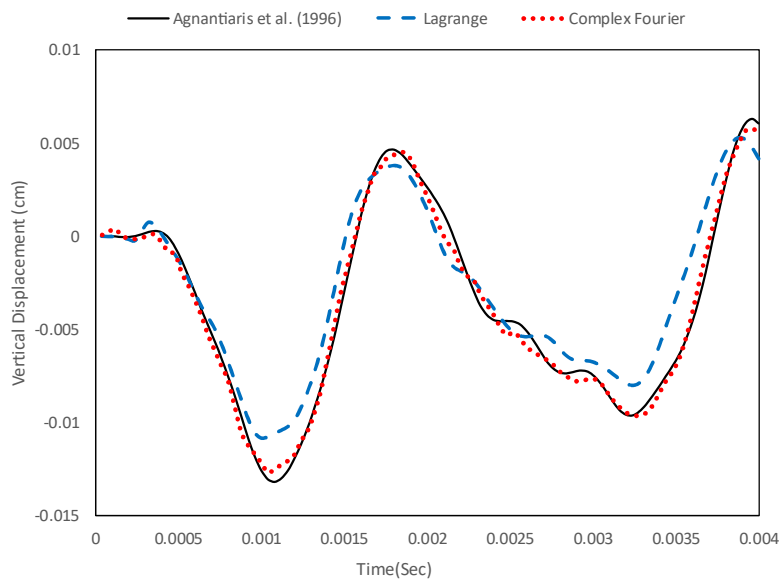
Fig. 6. The vertical displacement time history at point A.
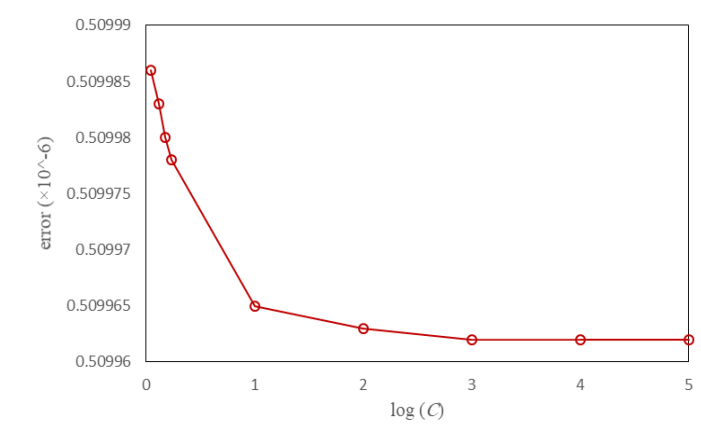
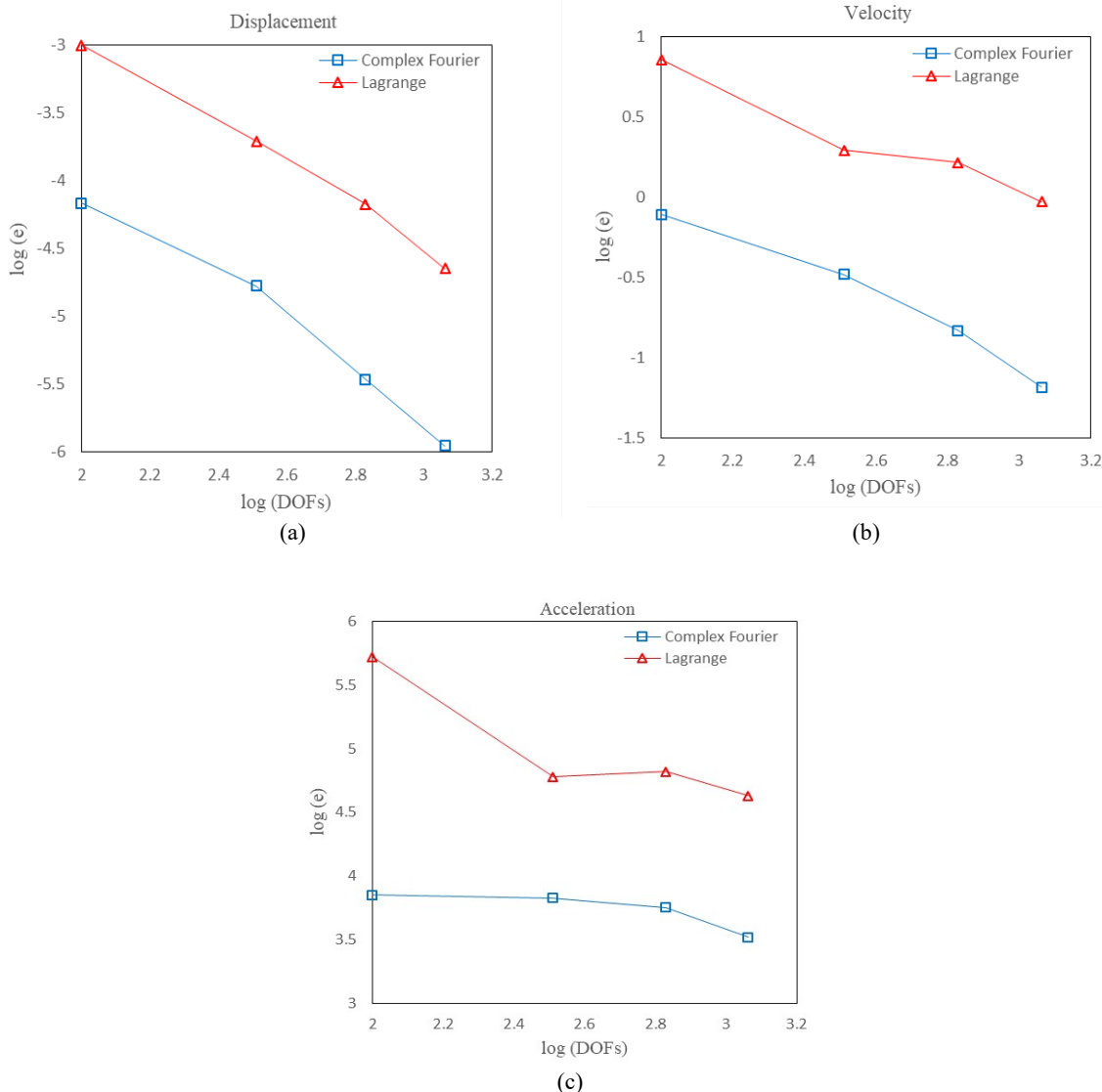**Fig. 7.** The effect of the penalty coefficient on the numerical results.

Fig. 8. Convergence rate diagram in: (a) displacement (b) velocity (c) acceleration

The results are compared with the high degree of freedom results of Agnantiaris et al (1996). As it is seen, the accuracy of the proposed method is much better than the classic Lagrange one. Fig. 7 shows the effect of the penalty coefficient (C) on the numerical results. The vertical axis shows the error which is defined as $\quad error = \sum_{i=1}^{m} (X_i - \bar{X}_i)^2 / m \quad$ in which, X_i and $\bar{X}_i$ denote the analytical (or high degree of freedom) and numerical solutions (for instance, the vertical displacement time

history of point A in this example), respectively; m is the number of points where the error is calculated. As shown in Fig. 7, the values of parameter C, which are bigger than unit, have no significant effect on the numerical results. The convergence rate for displacement, velocity and acceleration is plotted in Figs. 8a-8c. In this figure, the horizontal and vertical axes show the number of degrees of freedom in spatial domain (DOFs) and $e = error / \max(|X_i|)$ (error and X_i were defined above) in logarithmic scale, respectively. Fig 8. Shows that the convergence rate in both methods is almost the same, but it is clear that the proposed shape functions significantly improve the accuracy of Lagrange based space-time finite element method.

5.2 Infinite strip under loading with step time variation

An infinite strip with the width of 4 and infinite length is considered in the second example (Fig. 9a). The lower side of the strip is fixed and its higher edge is under uniform tensile traction. A hatched area with the dimensions of 2×4 whose left, right, and bottom edges are supported by pins is used as cross section in plane strain condition. The load magnitude is assumed to be unit and it is subjected suddenly to the strip (Fig. 9b). The material properties are: $E = 1 \times 10^5$, $v = 0.25$, and $\rho = 1$. The discretization of spatial-time domain is done using 4 elements in the width direction, 5 elements in the height, and 200 elements in time. Fig. 10 shows the normal stress time history of point A obtained by the proposed method and classic one and the results are compared with the analytical solution [Hamzehei-Javaran et al. (2011)]. As it is seen, significant false oscillations exist in the results of the classic Lagrange based TD-FEM method that are reduced extremely in the present method ones. In this example, due to the zero acceleration, the convergence rate is studied only for displacement and velocity. The results shown in Figs. 11a and 11b emphasize the superiority of the proposed shape functions. Also, similar to the example 1, the convergence rate of two methods is almost the same.
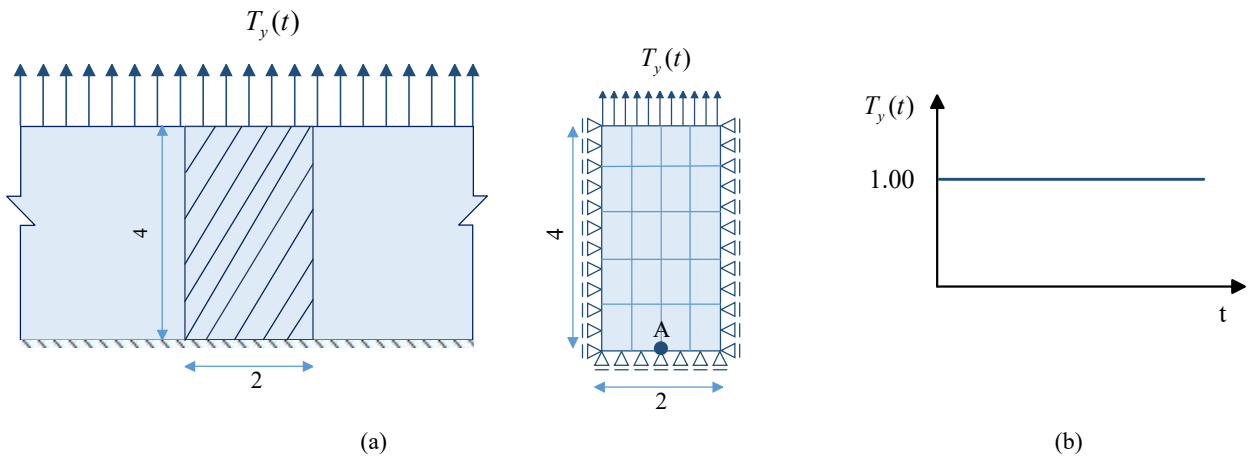

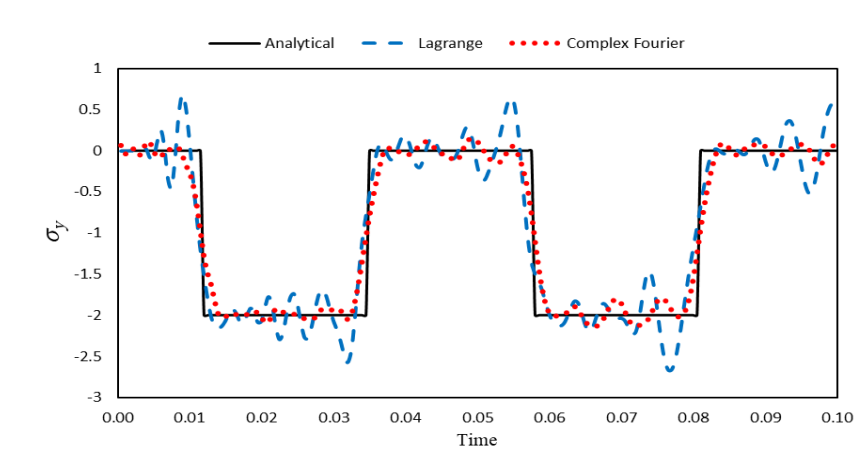**Fig. 9.** (a) Infinite strip and corresponding analytical model (b) Loading variation with respect to time

Fig. 10. Normal stress time history at point A.

5.3 Portal frame under dynamic lateral load

In the last example, the portal frame shown in Fig. 12a, which is under dynamic lateral load, is investigated. The frame material properties are $E = 2.4 \times 10^3$, $v = 0.2$, and $\rho = 1$. The spatial domain discretization is illustrated in Fig. 12b. The time domain is also discretized using 200 elements. The left edge of the frame is subjected to dynamic loading with the variation shown in Fig. 12c. In this example, the horizontal stress time history of point A as well as the horizontal displacement of point B are obtained from the proposed shape functions and classic Lagrange ones (Fig. 13). The results are compared with the high degree of freedom results of Brebbia and Nardini (2000) and Dominguez (1993). The superiority of the presented

method is clearly obvious from the results shown in the diagrams. Finally, the convergence rate diagram in displacement, velocity and acceleration are derived and the results are plotted in Fig. 14. Similar to the two previous examples, the convergence rate is almost the same for the proposed and traditional space-time finite element methods. Also, it is obvious that the proposed method leads to more accurate results in comparison with Lagrange based space-time finite element method.
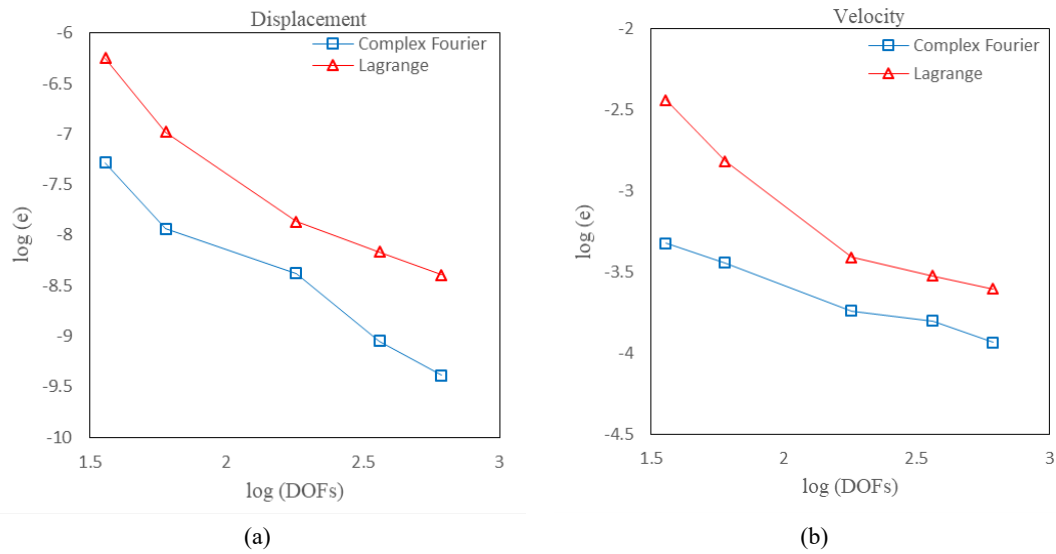

Fig. 11. Convergence rate diagram in: (a) displacement (b) velocity
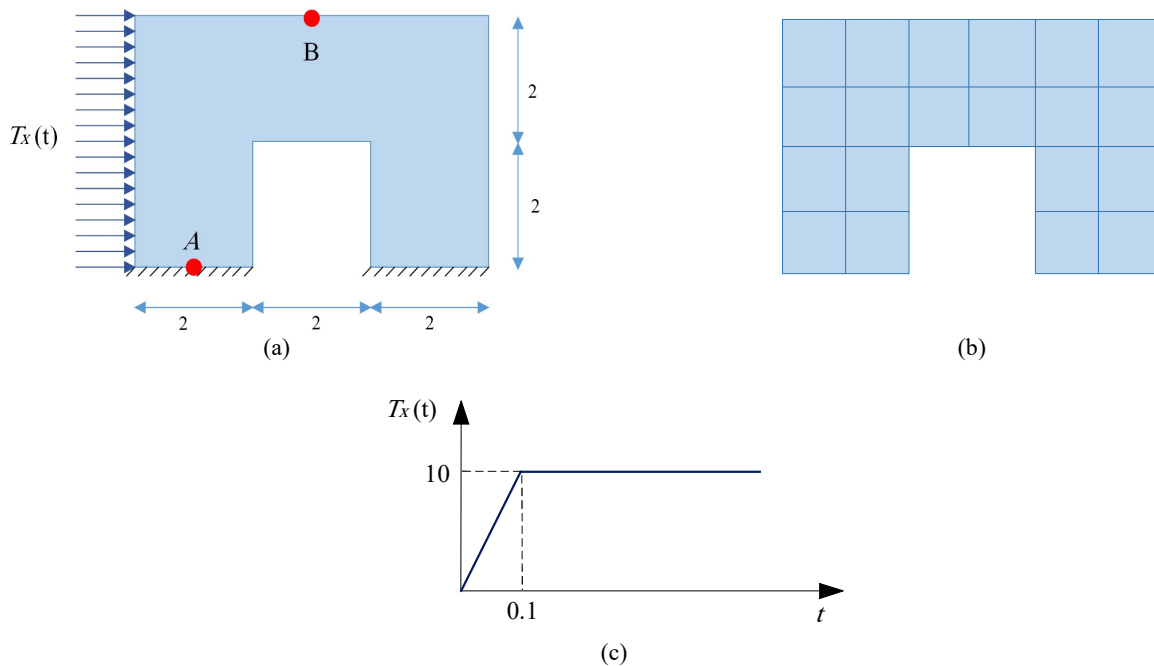

Fig. 12. (a) Geometry, boundary conditions, and loading of the portal frame (b) The discretization of spatial domain (c) The diagram of loading variation with respect to time

6. Conclusion

In this study, the time-discontinuous finite element method (TD-FEM) was chosen as a robust numerical method for solving two-dimensional elastodynamic problems. For this purpose, the complex Fourier functions were proposed as a new class of shape functions instead of classic Lagrange ones. The complex Fourier function consists of the combination of exponential and trigonometric functions in complex space as well as polynomial ones. Moreover, the oscillating and decaying features are among the suitable features of complex Fourier function that lead to having a suitable adaptation with the nature of dynamic waves in elastodynamics. For examining the accuracy and validity of the proposed method, three numerical examples were provided. It was clear from the results that the new time-discontinuous finite element formulation leads to more accurate and stable results than classic Lagrange-based TD-FEM one.
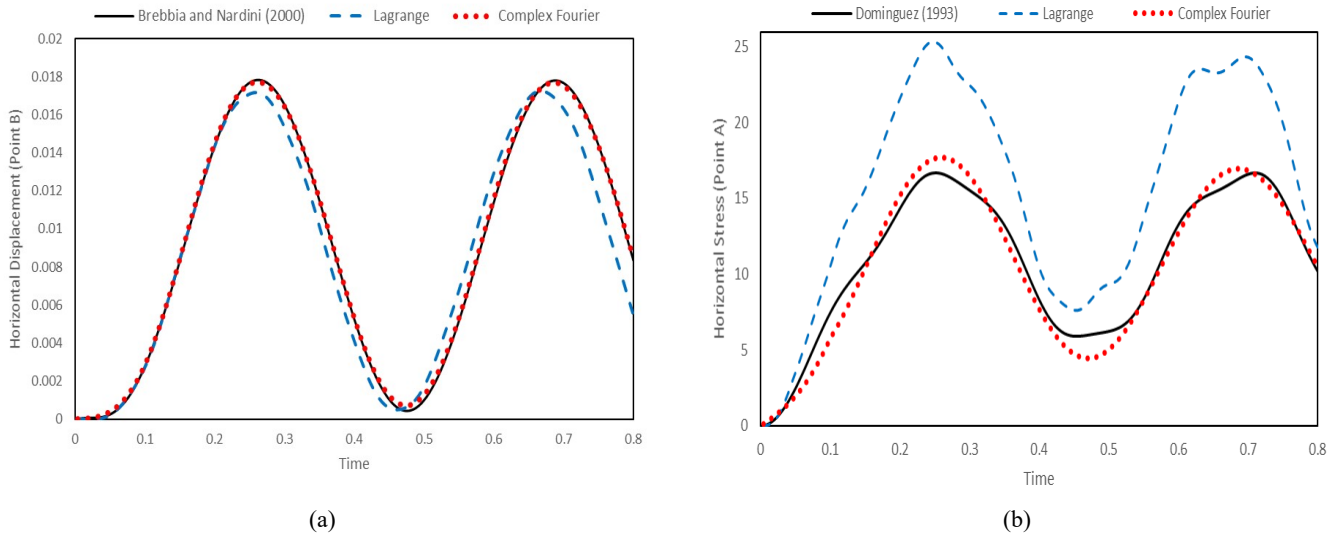
(a)   (b)

Fig. 13. (a) The horizontal displacement time history at point B (b) The horizontal stress time history at point A

(a)   (b)
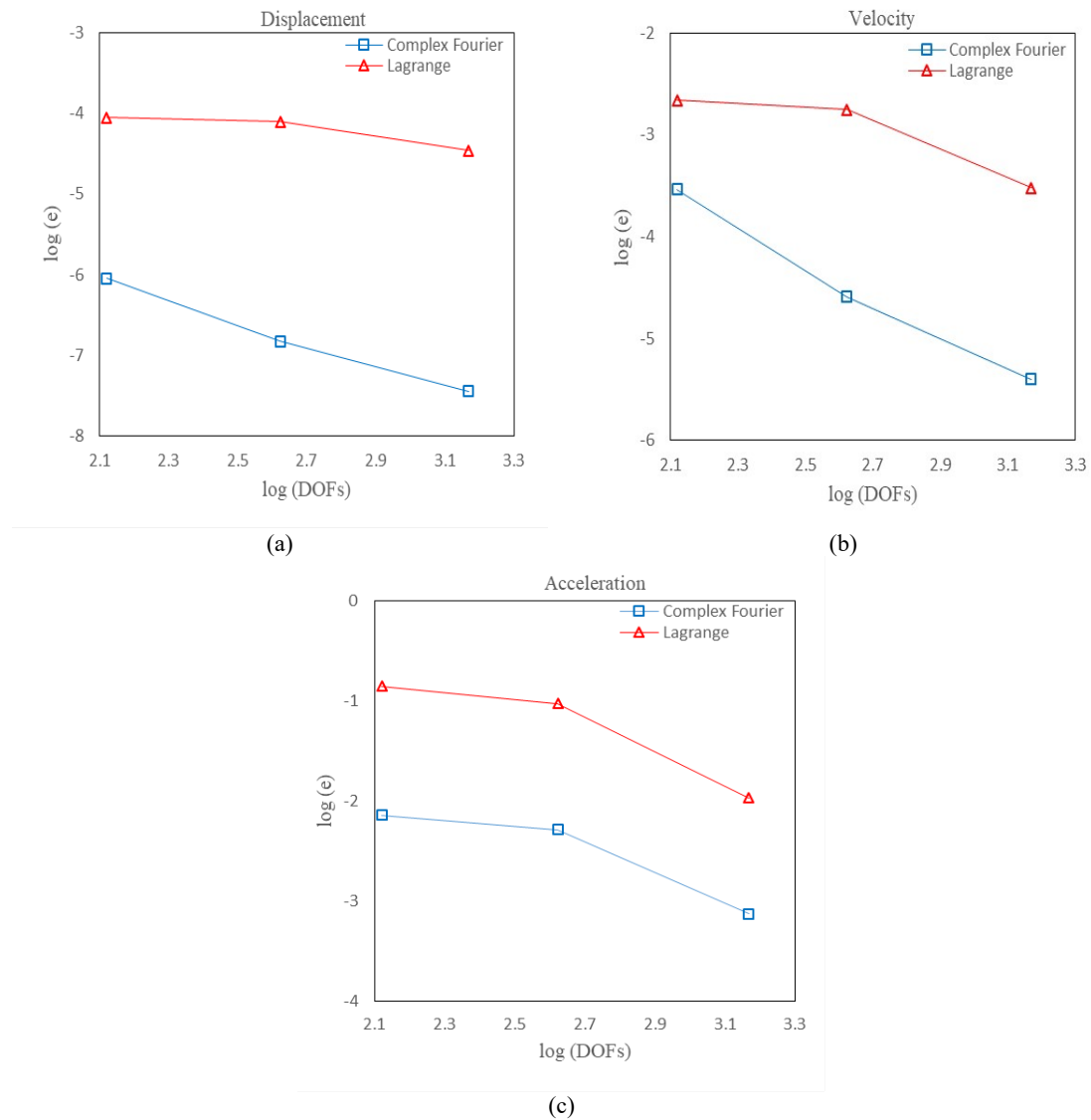

(c)

Fig. 14. Convergence rate diagram in the last example (a) displacement (b) velocity (c) acceleration

Conflict of Interest

The authors declare no conflict of interest.

References

Agnantiaris, J.P., Polyzos, D., Beskos, D.E., Some studies on dual reciprocity BEM for elastodynamic analysis, *Computational Mechanics*, 17 (1996) 270–277.

Aksoy, H.G., Şenocak, E., Discontinuous Galerkin method based on peridynamic theory for linear elasticity, *International Journal for Numerical Methods in Engineering*, 88(7) (2011) 673-692.

Argyris, J.H., Scharpf, D.W., Finite elements in time and space, *Nuclear Engineering and Design*, 10(4) (1969) 456-464.

Bathe, K.J, Baig, M.M.I., On a composite implicit time integration procedure for nonlinear dynamics, *Computers & Structures*, 83(31-32) (2005) 2513–2524.

Brebbia, C.A., Nardini, D., Dynamic analysis in solid mechanics by an alternative boundary elements procedure, *International Journal of Soil Dynamics and Earthquake Engineering*, 2 (1983) 228–233.

Bruch, J.C., Zyvoloski, G., Transient two-dimensional heat conduction problems solved by the finite element method, *International Journal for Numerical Methods in Engineering*, 8(3) (1974) 481-494.

Chung, J., Hulbert, G.M., A time integration algorithm for structural dynamics with improved numerical dissipation: The generalized-α method, *Journal of Applied Mechanics*, 60(2) (1993) 371–375.

Chien, C.C., Wu, T.Y., An improved predictor/multi-corrector algorithm for a time-discontinuous Galerkin finite element method in structural dynamics, *Computational Mechanics*, 25(5) (2000) 430-437.

Dominguez, J., *Boundary element in dynamics*. London: Computational Mechanics Publications, Southampton, Elsevier Applied Science, 1993.

Dyniewicz, B., Efficient numerical approach to unbounded systems subjected to a moving load, *Computational Mechanics*, 54 (2014) 321-329.

Fried, I., Finite-element analysis of time-dependent phenomena, *AIAA Journal*, 7(6) (1969) 1170-1173.

Fung, T.C., Higher-order accurate least-squares methods for first-order initial value problems, *International Journal for Numerical Methods in Engineering*, 45(1) (1999) 77-99.

Guo, P., Wu, W.H., Wu, Z.G., A time discontinuous Galerkin finite element method for generalized thermo-elastic wave analysis, *Acta Mechanica*, 225(1) (2014) 299-307.

Hamzehei Javaran, S., Khaji, N., Dynamic analysis of plane elasticity with new complex Fourier radial basis functions in the dual reciprocity boundary element method, *Applied Mathematical Modelling*, 38(14) (2014) 3641-3651.

Hamzeh Javaran, S., Khaji, N., Noorzad, A., First kind Bessel function (J-Bessel) as radial basis function for plane dynamic analysis using dual reciprocity boundary element method, *Acta Mechanica*, 218 (2011) 247-258.

Hilber, H.M., Hughes, T.J., Taylor, R.L., Improved numerical dissipation for time integration algorithms in structural dynamics, *Earthquake Engineering & Structural Dynamics*, 5(3) (1977) 283-292.

Hughes, T.J., Hulbert, G.M., Space-time finite element methods for elastodynamics: formulations and error estimates, *Computer Methods in Applied Mechanics and Engineering*, 66(3) (1988) 339-363.

Hulbert, G.M., Hughes, T.J., Space-time finite element methods for second-order hyperbolic equations, *Computer Methods in Applied Mechanics and Engineering*, 84(3) (1990) 327-348.

Hulbert, G.M., Time finite element methods for structural dynamics, *International Journal for Numerical Methods in Engineering*, 33(2) (1992) 307-331.

Khaji, N., Hamzehei Javaran, S., New complex Fourier shape functions for the analysis of two-dimensional potential problems using boundary element method, *Engineering Analysis with Boundary Elements*, 37(2) (2013) 260-272.

Lesaint, P., Raviart, P.A., On a finite element method for solving the neutron transport equation, in: C. de Boor ed., Mathematical Aspects of Finite Elements in Partial Differential Equations, Academic Press, NewYork, 89-123, 1974.

Lewis, D.L., Lund, J., Bowers, K.L., The space–time Sinc-Gallerkin method for parabolic problems, *International Journal for Numerical Methods in Engineering*, 24(9) (1987) 1629-1644.

Li, X., Yao, D., Lewis, R.W., A discontinuous Galerkin finite element method for dynamic and wave propagation problems in non-linear solids and saturated porous media, *International Journal for Numerical Methods in Engineering*, 57(12) (2003) 1775-1800.

Liu, Y., Li, H., He, S., Mixed time discontinuous space-time finite element method for convection diffusion equations, *Applied Mathematics and Mechanics*, 29(12) (2003) 1579-1586.

Nguyen, H., Reynen, J., A space-time least-square finite element scheme for advection-diffusion equations, *Computer Methods in Applied Mechanics and Engineering*, 42(3) (1984) 331-342.

Oden, J.T., A general theory of finite elements. II. Applications, *International Journal for Numerical Methods in Engineering*, 1(3) (1969) 247-259.

Peters, D.A., Izadpanah, A.P., Hp-version finite elements for the space-time domain, *Computational Mechanics*, 3(2) (1988) 73-88.

Petersen, S., Farhat, C., Tezaur, R., A space–time discontinuous Galerkin method for the solution of the wave equation in the time domain, *International Journal for Numerical Methods in Engineering*, 78(3) (2009) 275-295.

Reed, W.H., Hill, T.R., Triangular mesh methods for the neutron transport equation, Los Alamos Scientific Lab, N. Mex., USA, 1973.

Saedpanah, F., A posteriori error analysis for a continuous space-time finite element method for a hyperbolic integro-differential equation, *BIT Numerical Mathematics*, 53 (2013) 689-716.

Shao, H.P., Cai, C.W., A three parameters algorithm for numerical integration of structural dynamic equations, *Chinese Journal of Mechanical Engineering*, 5(4) (1988) 76–81.

Tamma, K.K., Zhou, X., Sha, D., A theory of development and design of generalized integration operators for computational structural dynamics, *International Journal for Numerical Methods in Engineering*, 50 (2001) 1619–1664.

Tang, Q., Chen, C.M., Liu, L.H., Space-time finite element method for schrödinger equation and its conservation, *Applied Mathematics and Mechanics*, 27 (2006) 335-340.

Varoglu, E., Liam Finn, W.D., Space-time finite elements incorporating characteristics for the burgers' equation, *International Journal for Numerical Methods in Engineering*, 16(1) (1980) 171-184.

Wang, J.G., Liu, G.R., On the optimal shape parameters of radial basis functions used for 2-D meshless methods, *Computer Methods in Applied Mechanics and Engineering*, 191(23) (2002) 2611-2630.

Wilson, E.L., Nickell, R.E., Application of the finite element method to heat conduction analysis, *Nuclear Engineering and Design*, 4(3) (1966) 276-286.

Zhou, X., Tamma, K.K., Design, analysis, and synthesis of generalized single step single solve and optimal algorithms for structural dynamics, *International Journal for Numerical Methods in Engineering*, 59 (2004) 597-668.

Zienkiewicz, O.C., Parekh, C.J., Transient field problems: Two-dimensional and three-dimensional analysis by isoparametric finite elements, *International Journal for Numerical Methods in Engineering*, 2(1) (1970) 61-71.

Zienkiewicz, O.C., Taylor, R.L., *The finite element method*, London: McGraw-Hill, 1977.

Zienkiewicz, O.C., A new look at the Newmark, Houbolt and other time stepping formulas, A weighted residual approach, *Earthquake Engineering & Structural Dynamics*, 5(4) (1977) 413-418.